Electronic Supplementary Material (ESI) for Chemical Communications.

Supplementary information

Nanoscale mapping of intrinsic defects in single-layer graphene using tip-enhanced Raman spectroscopy

Weitao Su[a, b, c†*], Naresh Kumar[b*], Ning Dai[c] and Debdulal Roy[b]

[a]Institute of Materials Physics, Hangzhou Dianzi University, 310018, Hangzhou, China
[b]National Physical Laboratory, Hampton Road, Teddington, Middlesex, TW11 0LW, UK
[c]Ningbo Institute of Materials Technology & Engineering, Chinese Academy of Sciences, 315201, Ningbo, China
[†]Email: suweitao@hdu.edu.cn
*These authors contributed equally to this work.

§1 TERS set-up

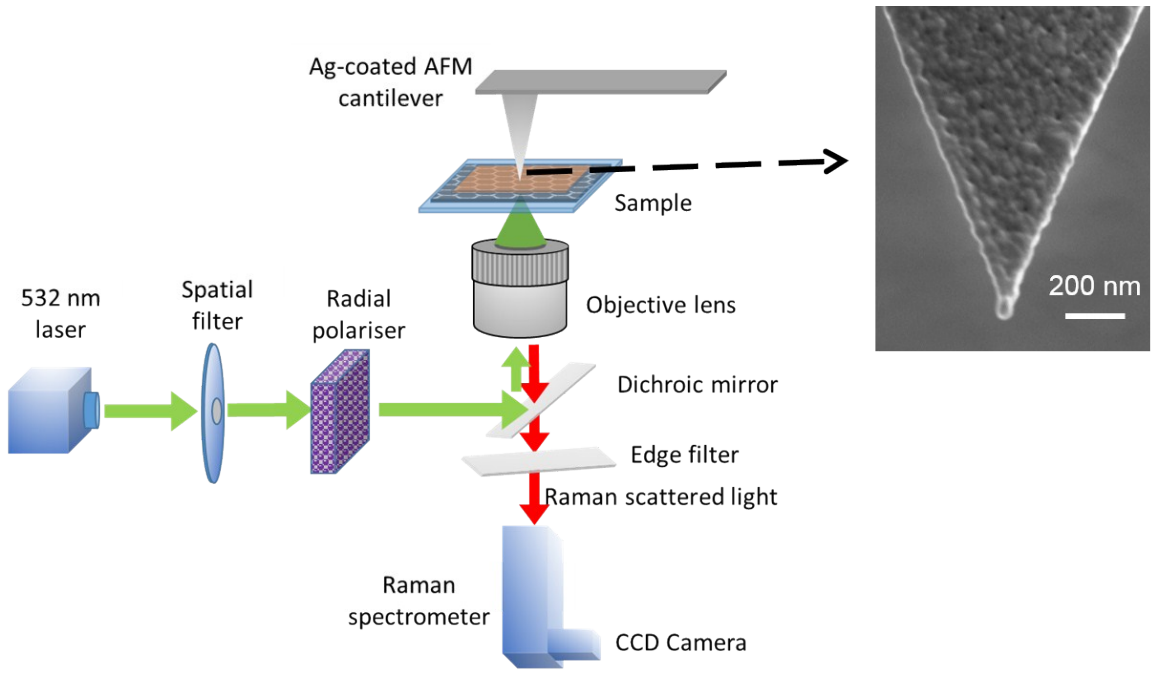

Fig. S1. Detailed schematic diagram of transmission-mode TERS setup used in this work. Single-layer graphene (grey honeycomb mesh) on a glass substrate (light blue) was used as the sample for TERS measurements. The inset shows the scanning electron microscope (SEM) image of the Ag-coated TERS tip used in this work.

TERS measurements were conducted in transmission mode on a bespoke system consisting of an inverted microscope (Ti-U Eclipse, Nikon, Japan) fitted with an atomic force microscope (AFM) (Combiscope, AIST-NT, The Netherlands) on top and a Raman spectrometer (iHR320, Horiba Scientific UK, Focal length: 320 mm) attached with an electron multiplying charge coupled device detector (Newton, Andor, Ireland). Gratings with 600 and 300 grooves/mm were used to measure the far field and near field spectra, respectively. Radially polarised 532 nm laser was focused onto the sample using a 100× 1.49 NA oil immersion objective lens (TIRF, Nikon, Japan).

§2 Individual confocal Raman maps and Raman spectra of single-layer and bilayer graphene

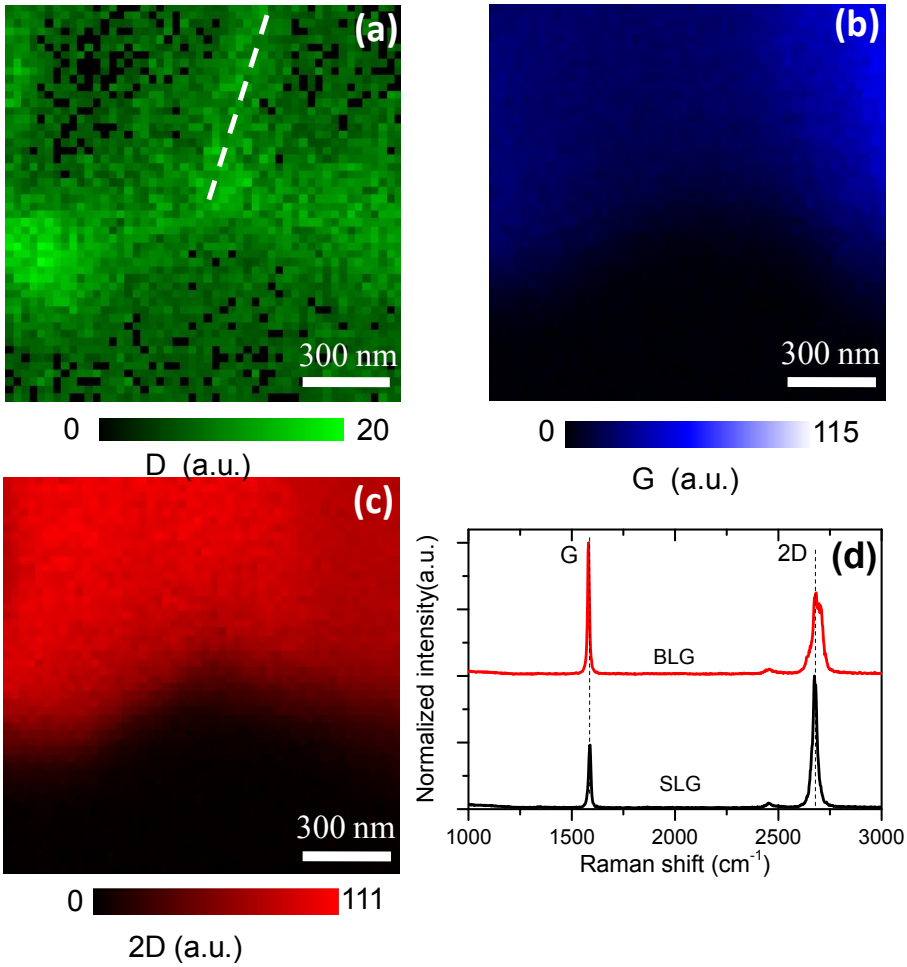

Fig. S2 Confocal Raman maps (60×60 pixels) obtained using the intensity of (a) D peak, (b) G peak and (c) 2D peak. Integration time per pixel: 1 s. (d) Confocal Raman spectra of single-layer (marked with circle in Fig. 1a) and bilayer (marked with a triangle in Fig. 1a) graphene. Integration time: 120 s.

Individual confocal Raman intensity maps of D, G and 2D Graphene Raman peaks are shown in Fig. S2a-2c, respectively. In Fig. S2d, two Raman spectra measured from the single-layer and bilayer graphene areas marked in Fig. 1a are shown. Single-layer graphene can be identified using the width of 2D peak. Using a single Lorentz peak fitting, the half-width of 2D peaks are calculated to be 27 cm^{-1} and 59 cm^{-1} for single-layer and bilayer, respectively.

§3 Identification of the type of line defect

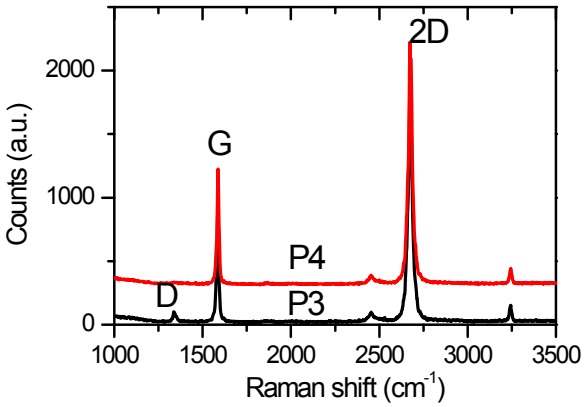

Fig. S3 Far-field Raman spectra of single-layer graphene with (at position P3 marked in Fig. 1c) and without (at position P4 marked in Fig. 1c) line defect.

Table S1. Peak parameters calculated from the Raman spectra measured at the positions of line defect and away from line defect on single-layer graphene

	I_D	I_G	W_G	I_{2D}	W_{2D}	I_D/ I_G	I_G/ I_{2D}
Away from line defect	9	952	11.3	1889	23.98	0.010	0.50
At line defect	73	869	11.9	1808	25.65	0.084	0.48

Because no contrast can be observed at the line defect position in AFM topography, phase or lateral force images shown in Fig. 1a, 1b and 2a, respectively, the possibility of structural defects such as voids or small edges is ruled out. Far field Raman spectra of single-layer graphene measured at the position of line defect (P3) and away from the line defect (P4) are shown in Fig. S3. The calculated peak parameters of the corresponding D, G and 2D peaks are shown in Table S1. It can be noted that the I_D/ I_G ratio at line defect is nearly 8.5 times stronger than that of single-layer graphene region without defect, although I_G/ I_{2D} slightly decreases. Furthermore, both G and 2D peaks are broadened and redshifted. These features indicate the presence of disordered sp^2 carbon and tensile strain at the position of the line defect. Therefore, the observed line defect most likely consists of a mixture of disordered sp^2 carbon and linear dislocation induced strain, rather than structural defects.

§4 TERS maps of D, G and 2D Raman bands and calculation of TERS spatial resolution

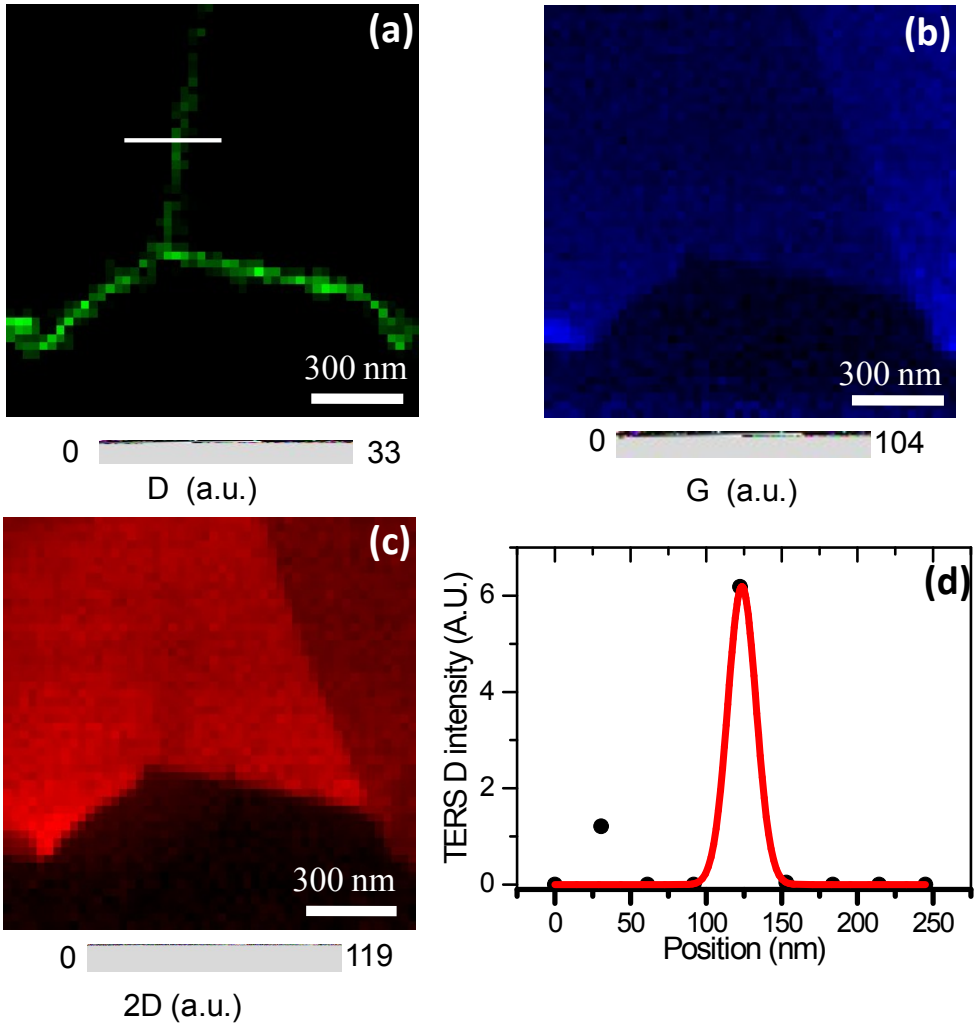

Fig. S4 TERS intensity maps (50×50 pixels) of (a) D, (b) G and (c) 2D peaks. Integration time per pixel: 1 s. (d) Gaussian fitting of line profile marked position in S3a. TERS spatial resolution is estimated from the full width at half maximum (FWHM) to be 20 nm.

It should be noted that in Fig. 2b, TERS mapping is performed in a 1500 × 1500 nm^2 area using 50 × 50 pixels. Therefore, the nominal pixel size (step size) in the TERS map is 30 nm. Furthermore, in the D-peak TERS map in Fig S4a, D-peak is observed only along a line consisting of single pixels with a size of 30 nm. This implies that in this TERS map the spatial resolution is limited only by the pixel size and should be much less than 30 nm. Therefore, the 20 nm FWHM of the Gaussian fit to the intensity profile shown in Fig. S4d is a reasonable estimate of the spatial resolution of the D peak TERS map.

The spatial resolution of a TERS map depends two factors: (a) Distance between the tip and the sample and (b) The radius of the TERS tip. It has been previously demonstrated that the spatial resolution is similar to the radius of the tip apex when the TERS tip is at a distance of < 2 nm to the sample for e.g. in contact mode AFM, which has been used in this work[1-3]. The estimated spatial resolution of 20 nm is consistent with the radius of ≈ 25 nm measured from the SEM image of the TERS tip shown in Fig S1. Furthermore, This estimate is also similar to the

spatial resolution reported previously on other samples obtained using the TERS probes prepared using exactly the same procedure in our laboratory such as single-layer graphene (Spatial resolution 18 nm: Su *et al.*[4]; Spatial resolution 24 nm: Mignuzzi *et al*[5].), single-layer MoS_2 (Spatial resolution 20 nm)[6] and photocatalytic reaction on silver catalysts (Spatial resolution 20 nm)[7].

§5 Second electromagnetic enhancement of the Raman modes of graphene in the near-field

In this work, the TERS enhancement factor and contrast follow the sequence D>G>2D. This selective enhancement can indeed be well interpreted by second electromagnetic enhancement described by Yamamoto *et al*[8].. According to this theory, the selective enhancement of Raman modes of a sample is strongly dependent on their separation from the resonant energy of tip. The closer the wavelength of a Raman mode to the resonant wavelength of tip, the stronger the enhancement of this Raman mode. This implies that the law of TERS enhancement being proportional to the fourth power of the near-field intensity of electrical field may not strictly hold true for Raman modes with wavelengths far from the excitation wavelength and hence needs to be revised.

The electromagnetic resonant wavelength of the silver tip can be obtained from the photoluminescence (PL) spectrum of the tip measured on a blank glass coverslip as shown in Fig. S5. It can be noted in Fig. S5 that the position of PL peak in the spectrum lies at a shorter wavelength than the excitation laser (532 nm, at zero Raman shift). However, the energy of Raman D, G and 2D photons fall at the low energy slope of the resonant curve of the tip. The energy difference between the resonant peak of tip and different Raman photons follows the sequence D<G<2D. Therefore, the plasmonic enhancement of the Raman modes follows the sequence D>G>2D implying that the law of TERS enhancement being proportional to the fourth power of the near-field intensity of electrical field doesn't apply equally to the D, G and 2D Raman modes.

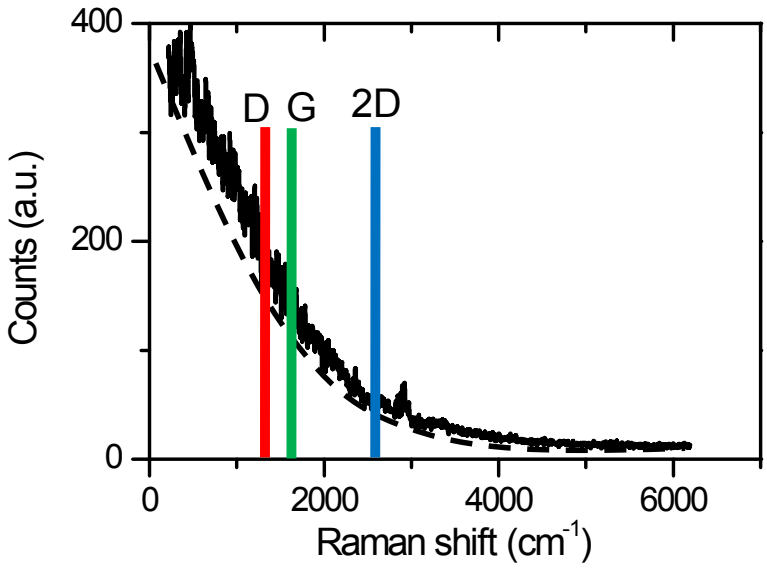

Fig. S5 Spectrum of Ag-coated TERS tip used in this work measured on a glass substrate without graphene. The PL band of the tip is indicated by the dashed black line. The peak positions of D, G and 2D bands are shown by the red, green and blue solid lines, respectively.

§6 Comparison of TERS enhancement factor obtained in this work with the previous reports

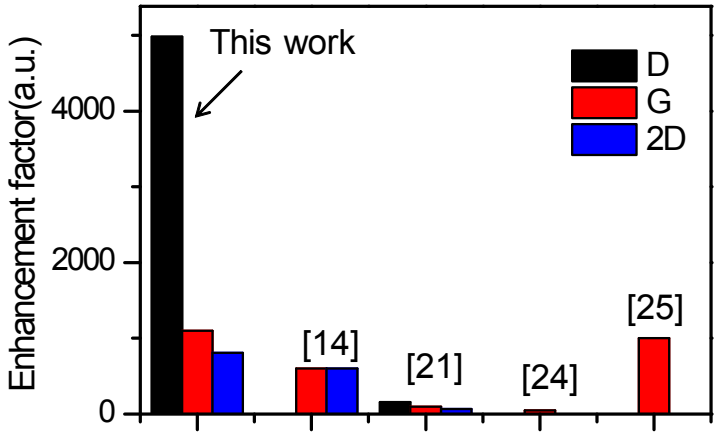

Fig. S6 Comparison of the TERS enhancement factor of the Raman peaks in single-layer graphene obtained in this work with the previous reports. The reference numbers correspond to the references cited in the main text.

In Fig. 3c, TERS contrast obtained in this work has been compared with the previous reports. In Fig. S6, we present the comparison of the TERS enhancement factor with the enhancement factor reported in previous reports. The G peak enhancement factor obtained in this work is comparable to that obtained by Suzuki *et al.* measured using a side illumination TERS set-up in non-gap mode[9]. However, it can be noted that our D-peak TERS enhancement factor is significantly higher than that reported values measured in transmission as well as side illumination TERS modes. We believe that the strong signal enhancement observed in this work can be attributed to the efficient excitation of a strong localised surface plasmon (LSP) resonance at the tip-apex.

References

1. N. Behr and M. B. Raschke, *J. Phys. Chem. C*, 2008, **112**, 3766-3773.
2. B. Pettinger, B. Ren, G. Picardi, R. Schuster and G. Ertl, *J. Raman Spectrosc.*, 2005, **36**, 541-550.
3. Z. Yang, J. Aizpurua and H. Xu, *J. Raman Spectrosc.*, 2009, **40**, 1343-1348.
4. W. Su and D. Roy, *J. Vac. Sci. Technol. B*, 2013, **31**, 041808.
5. S. Mignuzzi, N. Kumar, B. Brennan, I. S. Gilmore, D. Richards, A. J. Pollard and D. Roy, *Nanoscale*, 2015, **7**, 19413-19418.
6. W. Su, N. Kumar, S. Mignuzzi, J. Crain and D. Roy, *Nanoscale*, 2016, **8**, 10564-10569.
7. N. Kumar, B. Stephanidis, R. Zenobi, A. J. Wain and D. Roy, *Nanoscale*, 2015, **7**, 7133-7137.
8. Y. S. Yamamoto and T. Itoh, *J. Raman Spectrosc.*, 2016, **47**, 78-88.
9. T. Suzuki, T. Itoh, S. Vantasin, S. Minami, Y. Kutsuma, K. Ashida, T.-a. Kaneko, Y. Morisawa, T. Miura and Y. Ozaki, *Phys. Chem. Chem. Phys.*, 2014, **16**, 20236-20240.